Available online at www.sciencedirect.com

ScienceDirect

Energy Procedia 49 (2014) 1592 – 1602

Energy Procedia

SolarPACES 2013

Dynamic simulation of a 1MWe concentrated solar power tower plant system with Dymola®

J.B.Zhang[a,] *, J.C. Valle-Marcos[a], B. El-Hefni[b] , Z.F. Wang[c], G.F. Chen[a], G.C. Ma[c], X. Li[c], R. Soler[d]

[a]*EDF China R&D Center, China Division, EDF Asia Pacific Branch, Beijing 100005, China.*
[b]*EDF R&D, EDF, Chatou 78401, France*
[c]*The Key laboratory of Solar Thermal Energy and Photovoltaic System, Institute of Electrical Engineering, Chinese Academy of Sciences, Beijing 100190, China*
[d]*EDF R&D, EDF, Clamart 92140, France*

Abstract

This paper presents a first vertion of a dynamic model of the 1 MWe Central Receiver System demo plant at Badaling in Beijing with the purpose of improving the performance and reliability of the CSP technology deployed at this plant using dynamic modelling by Dymola® software in the frame of cooperation between EDF R&D and IEECAS (Institute of Electrical Engineering of the Chinese Academy of Sciences). This dynamic model is capable of simulating the dynamic behavior of the entire CSP plant, covering the heliostat field, the superheated steam cavity receiver, the thermal storage system and the power block. In order to validate the model, the demo plant operation data is used. The recorded evolution of the different process parameters during the operation is compared to the results predicted by the dynamic model. According to the results obtained from the operation, the simulation predicts fairly well the main process parameters. The predicted trend of the dynamic behavior of the system is also satisfactory. The results show that the model could be used to support the operation of the entire solar thermal power tower system and help improve the performance of the CSP technology deployed at Badaling.

Selection and peer review by the scientific conference committee of SolarPACES 2013 under responsibility of PSE AG.
Final manuscript published as received without editorial corrections.

Keywords: Badaling CSP plant, dynamic Dymola® model, “Thermosyspro" library, campaign operation

* Corresponding author. Tel.: +861058681359; fax:+861058681355
E-mail address: jinbai.zhang@edf.fr

Selection and peer review by the scientific conference committee of SolarPACES 2013 under responsibility of PSE AG.
Final manuscript published as received without editorial corrections.
doi:10.1016/j.egypro.2014.03.168

1. Introduction

In the frame of Chinese CSP development program, a 1MWe tower solar thermal demo plant was built in Badaling as the key project of the 11th Five-Year Plan of China National Hi-Tech R&D (863 Plan). It is owned and operated by the Institute of Electrical Engineering of the Chinese Academy of Sciences (IEE-CAS). Since 2012, EDF R&D has been cooperating with IEECAS in the frame of a joint R&D program aiming at improving the performance and reliability of the CSP technology deployed at this demo plant by using dynamic modelling method.

Many works have been done on the CSP system simulation for the past three decades. Manteau (1) as well as Ferriere and Bonduelle (2) developed a storage model in 1978 and a receiver model, respectivly. Both studies were done based on the earliest molten salt CSP tower plant, Thémis, in France. Xu et al. (3) and Yu et al. (4) also simulated the key components performance of Badaling demo plant such as the storage system, solar field and central receiver.

In this paper, a first version of a dynamic model is built using Dymola® software and the "Thermosyspro" library of Modelica models built initially by EDF R&D for conventional plants. The dynamic model is capable of simulating the dynamic behaviour of the entire CSP plant, covering the heliostat field, the superheated steam cavity receiver, the thermal storage system and the power generation block. Besides, a series of campaigns in the demo plant have been scheduled, in order to recover enough feedback from experiences and operational data which can be used to validate our model. According to the results obtained from the operation, the simulation predicts fairly well the main process parameters. The predicted trend for the dynamic behaviour of the system is also satisfactory. The result shows the model can provide good references for the operation of the entire plant and can be used to improve the performance of the CSP technology deployed in Badaling.

Nomenclature

$C_e.h$	Fluid specific enthalpy at the inlet
$C_s.h$	Fluid specific enthalpy at the outlet
cpw	Wall specific heat capacity
D	Internal pipe diameter
DNI	Incident energy
E	Corrective term for hcl
e	Wall thickness
h_{cl}	Convective heat transfer coefficient for the liquid fraction
h_{cv}	Convective heat transfer coefficient for the vapor fraction
h_{eb}	Convective heat transfer coefficient for vaporization
h_i	Fluid specific enthalpy at the inlet; Convective heat transfer coefficient
hiCorr	Corrective term for the convective heat transfer coefficient
H_s	Enthalpy of superheated steam
H_w	Enthalpy of inlet water
k_v	Thermal conductivity for the vapor
L	Pipe length
M	Wall mass
N_h	Number of heliostats connected
Pr_v	Fluid Prandtl number for the vapor
Q	Mass flow rate through the turbine
Q_s	Superheated steam flow rate
Q_w	Inlet water flow rate
Re_v	Reynolds number for the vapor
S	Corrective term for nucleation removal
S_h	Surface of one heliostat
S_i	Internal heat exchange area
T	Fluid temperature

T_m	Average wall temperature
T_i	Inside wall temperature
T_o	Outside wall temperature
W	Mechanical power produced by the turbine
W_{fric}	Power losses due to hydrodynamic friction
W_i	Thermal power transferred from the metal to the work fluid
W_o	Thermal power transferred from the incident energy to the wall
xb_1	Min value for vapor mass fraction
xb_2	Max value for vapor mass fraction
x_v	Vapor mass fraction
λ	Wall thermal conductivity

2. Description of system

The Badaling demo plant mainly consists of an heliostat field, a receiver system, a thermal storage system and a power generation system. The heliostat field is composed by 100 sun-tracking heliostats, each with an area of 100 m^2. The dimension of each heliostat, which consists of 64 small square mirror elements, is 10 × 10 m, mounted on a 6.6 m high steel pillar. The incident solar rays are concentrated and reflected into a cavity-type receiver, which will be located at 78 m above the ground. Most of the incident energy reflected by the heliostats is absorbed by the receiver through the 5 × 5 m^2 aperture, with a maximum production capacity of 8.7 t/h of superheated steam. The cavity receiver mainly consists of seven evaporating panels set in parallel, four superheaters set in series and a drum. During the operation, the feed water is firstly pumped into the drum then it enters the evaporating panels via the downcomers and circulation pump. After the projection of heliostats, the incident solar energy is absorbed by the water through the exchanged heat through the metal wall of the panels. The steam and water are separated in the drum then the steam flows into the superheaters to absorb the energy, while the separated water will be recirculated to the evaporating panels. Finally, the superheated steam is produced and feeds the steam turbine. The steam from the turbine is condensed in a condenser then the water flows back to the deaerator before it is pumped back to the receiver (Fig. 1).

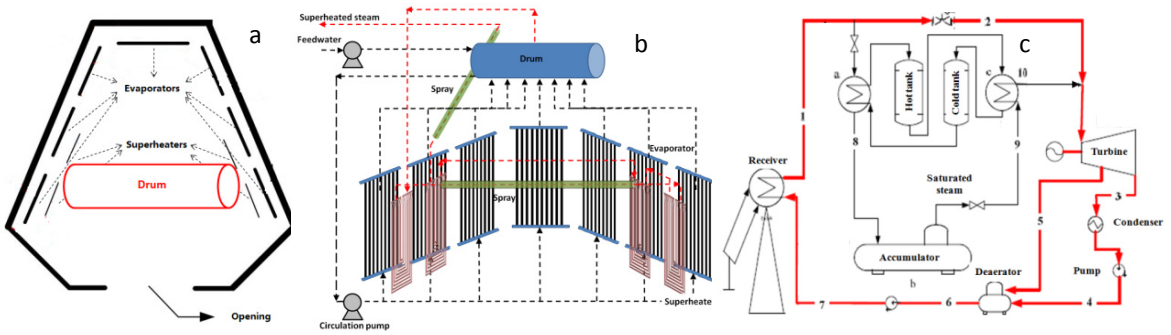

Fig. 1. (a) Vertical view of the cavity receiver; (b) Schematic of the water/steam circulation in the cavity receiver; (c) Flow chart of power plant without storage system.

3. Description of campaign

A demo plant campaign consists in the operation of the plant during a period of time and according to a sequence of predefined operation instructions, with the aim of obtaining operation data that can be used to carry out the validation test with the Dymola® dynamic model. The campaign considered in this study was carried out in August 29th 2012 from 9h00 to 16h20. Since the thermal storage system was not available at that time, this campaign

focused on the heliostat field, receiver system and power block. The weather condition was monitored by an on-site meteorological station. Passage of clouds was noticed, which influenced significantly the DNI evolution. Besides, a bad condition was created on purpose by using only 60-70% of the heliostats and leaving the dust deposited on the mirrors without cleaning which lead to an important reflectivity efficiency reduction. In the near future, the results of this campaign will be used as a reference to draw a comparison with the feedback of another test campaign which will be carried out with better initial conditions in terms of heliostat reflectivity.

4. Model development

During the development of the global model, some specific modules such as the heliostat field or the solar receiver, were specifically developed in the frame of this work, based on the characteristics provided by IEE-CAS; other conventional power plant modules, already existing in the "ThermoSysPro" library, such as the pumps, valves, and heat exchangers, were used in the global CSP model, either directly or after modification. The different equipment modules are based on the mass, energy and momentum conservation equations as well as on the basic relationships of solar irradiation, heat transfer, thermodynamics, and fluid mechanics. Different equipment modules are linked together, depending on the heat transfer, energy conversion, and system structures.

4.1. Solar field and heliostat model

The solar field model is composed of two essential parts: the solar field layout calculation and the heliostat model. The design of the heliostat field layout is based on the radial staggering method (5) with the aim of maximizing its efficiencies. The losses of the heliostats field mainly include the losses relating to cosine factor, shading, blocking, atmospheric attenuation, and spillage. For the unimpeded movement of the heliostats of 10m×10m, the characteristic diameter of the heliostat using the design work is given by 16m, which is larger than its diagonal. The radius of the first heliostat ring in the field, defined as an essential ring, is equal to the aim point height. The radius of other rings is theoretically calculated based on no blocking loss. While the radial distance between adjacent rings is then adjusted to allow passage of cleaning truck (6). The heliostat model is composed of two main submodels: The solar energy flux submodel and the receiver heat flux distribution submodel. Main assumptions made concerning the solar energy flux submodel are:

- The center of each heliostat is assumed to coincide with the highest point of its steel pillar.
- The heliostat tracking error and the mirror caused by the external environment conditions (e.g. sudden strong wind) are neglected.

In the current state of development, the first submodel is completed, in which the radiation evolves with time during the day and all along the year, considering the elevation and altitude angle of the sun, pitching and deflection angle of the heliostat, as well as relative location between the heliostat and the receiver. The model can determine the efficiency of each heliostat and the values of solar radiation reflected from each heliostat and arriving into the receiver. The input data is composed by DNI evolution, heliostat coordinate and heliostat design parameters. The DNI data is measured by the meteorological station during the campaign. The coordinates of the heliostats are calculated with the layout of the solar field mentioned above.

The second submodel (heat flux distribution) is based on the tracing of the intersection points of reflection rays from the entire heliostat field on a single aiming point which is centered in the aperture. The concentrated solar flux distribution on the receiver often presents a Gaussian-like distribution shape with a high peak flux density in the center. The aim of this model is to define the incident heat distribution on evaporators and superheaters. Currently, a simplified heat distribution module is used to define the ratio of incident heat on each component in the receiver, based on the results obtained with Soltrace®, developed by NREL. More precisely, the inner surface is divided into several areas in order to define the heat flux distribution in the receiver and calculate the fraction of flux received by each evaporator and superheater panel.

4.2. Receiver and power block

Most of the incident energy reflected by the heliostats is absorbed by the receiver, where the water is preheated and evaporated in the evaporators and the steam is then superheated in the superheaters. In this process, two types of heat transfer are noticed including convection heat transfer in single-phase fluid and two-phase fluid, leading to a different heat transfer coefficient between the working fluid and metal wall. Several assumptions are made:

- Axial heat transfer is neglected.
- Heat loss that occurs from the tube to the atmosphere is not considered.
- The radiative heat transfer between tubes and between heat exchangers is not taken into account.
- Besides the evaporators and superheaters, the thermal inertia of other parts of the receiver body is not considered.
- The leak of working fluid in the pipes is neglected.
- It is considered that there is no trace of water at the superheater inlet.

The model is basically composed of ThermoSysPro's exchangers, wall and heat source modules, in which the two phase and one phase exchangers are applied for evaporator and superheater, respectively. The input power is determined by the energy output of the heliostat module in our case. The characteristics of the exchanger wall module are kept consistent with the exchanger, such as the length, the number and the diameter of the pipes in the exchanger (Fig. 2).

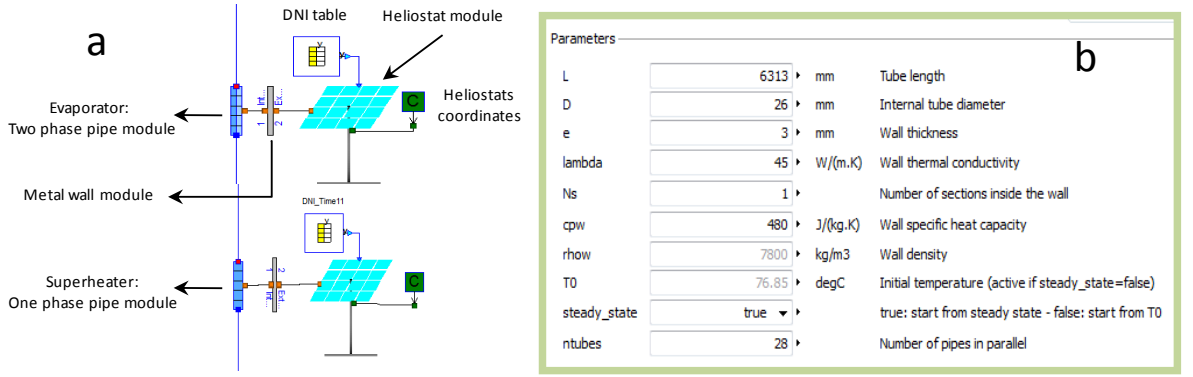

Fig. 2. (a) Components of evaporator and superheater; (b) input data for the wall module.

The thermal inertia is also taken into account and calculated by Eq. 1.

$$M \times cpw \times \frac{dT_m}{dt} = W_0 - W_i \tag{1}$$

The heat transfer between the outside wall and the average metal wall as well as that between the average metal wall and the inside wall is determined by:

$$W_0 = \frac{2 \times \pi \times L \times \lambda \times (T_0 - T_m)}{\log(1 + \frac{e}{e + D})} \tag{2}$$

$$W_i = \frac{2 \times \pi \times L \times \lambda \times (T_m - T_i)}{\log(1 + \frac{e}{D})} \tag{3}$$

Then, the heat transfer from the inside wall to the liquid is calculated by:

$$W_i = h_i \times S_i \times (T_i - T) \tag{4}$$

The thermal inertia is also considered by:

$$M \times cpw \times \frac{dT_m}{dt} = W_o + W_i$$

The calculation of the convective heat transfer coefficient h_i depends on the flow pattern, which is different between evaporator and superheater. Two flow patterns are considered in the modeling progress. The heat transfer coefficient in single-phase fluid forced flow is calculated by using directly the Dittus-Boelter formula:

$$h_i = \frac{hiCorr \times 0.023 k_v}{D} \times \mathrm{Re}_v^{0.8}\ \mathrm{Pr}_v^{0.4} \tag{5}$$

For the heat transfer coefficient in two-phase fluid forced flow, it depends on the vapor mass fraction in the pipe shown as follows:

$$\begin{aligned} h_i &= (1 - \frac{x_v}{xb_1}) \times h_{cl} + (\frac{xv}{xb_1}) \times (E \times h_{cl} + S \times h_{eb}) && x_v < xb_1 \\ h_i &= \frac{x_v - xb_2}{1 - xb_2} \times h_{cv} + \frac{1 - x_v}{1 - xb_2} \times (E \times h_{cl} + S \times h_{eb}) && x_v > xb_1 \\ h_i &= E \times h_{cl} + S \times h_{eb} && xb_1 < x_v < xb_2 \end{aligned} \tag{6}$$

The drum is located at the top of the receiver and acts as a key component of buffer and steady pressure together with an additional feed water source and backup tank, also taken into account in the model. According to the structure and working principle, the drum model is divided into the vapor region and liquid region. The steam flow rate and the recirculation rate are determined as a function of the related valves opening and pressure gradient between up and down stream of the valves. In the model, the heat exchange between the drum wall/downcomers and the outside is not considered and there is no phase change in the downcomer of the drum. In the model, the dimension of the drum, the characteristics of the metal wall and the heat exchange coefficient between different phases can be defined.

The conventional power block consists of a steam turbine, a generator and a condenser, for which the modules are available in the library “ThermoSysPro”. The mechanical power produced by the turbine is obtained by:

$$W = Q \times (C_e.h - C_s.h) \times (1 - W_{fric}) \tag{7}$$

5. Results and discussion

The operation data from the campaign mentioned above is compared to the model results obtained when applying the same DNI as observed that day. The results obtained by the solar field layout model are also discussed.

5.1. Solar field and heliostat model

Based on the layout obtained from the theoretical design model, some parameters such as the radial distances between adjacent rings were modified in order to better represent the real layout, for which the heliostat maintenance related constraints in terms of accessibility to each heliostat needs to be considered. The coordinates are then obtained from the model and used in Soltrace® to calculate the heat distribution in the receiver (Fig. 3). Soltrace® has previously been successfully used for simulating the Thémis solar field and heat distribution in the receiver (7).

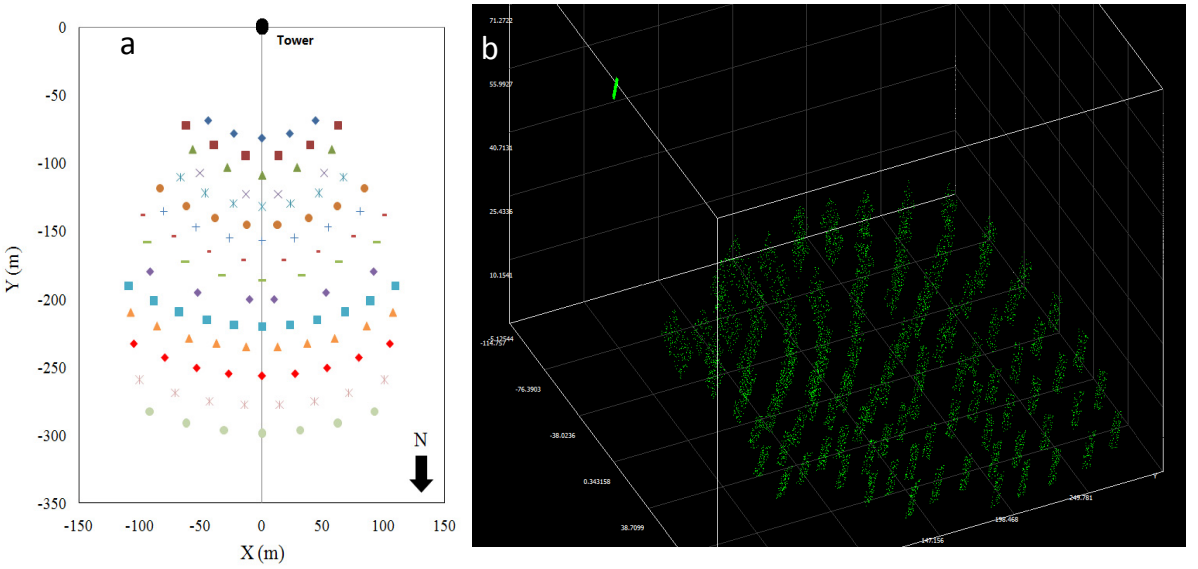

Fig. 3. (a) Solar field layout result by model; (b) Calculation of heat distribution in the receiver.

The heliostat module of the Dymola® model uses as input data the measured DNI during the campaign and the coordinates of heliostats, in order to predict the thermal power arriving at the receiver from each heliostat (Fig. 4 a).

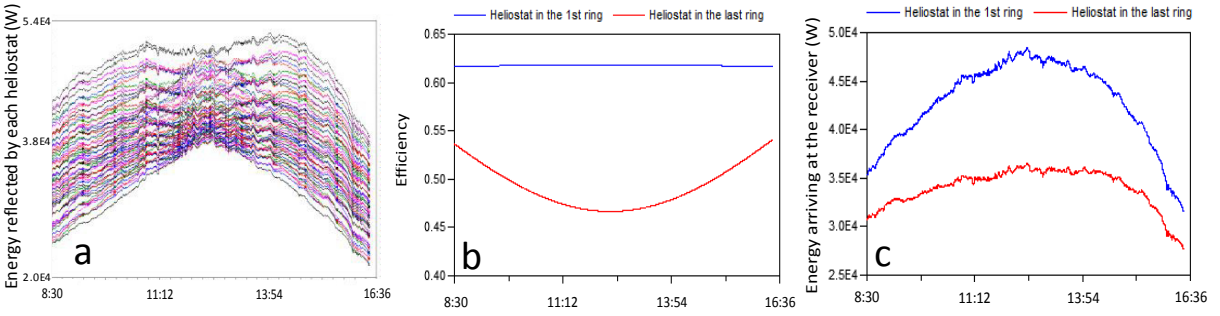

Fig. 4. (a) Energy arriving at the receiver reflected by each heliostat; (b) Difference of heliostat efficiency and (c) energy arriving at the receiver reflected by each heliostat between heliostats located in the 1st ring and the last ring, respectively.

The difference in flux contribution between different heliostats is due to the evolution of efficiency depending on the heliostat location and distance to the receiver. E.g. the difference in heliostat efficiency between a heliostat in the first and last ring varies between 8.0 and 15.2 points along the day, which causes a difference in reflected energy of up to 25% (Fig. 4 b and c). The efficiency of the light-heat transfer system including the solar field and the receiver

is also an essential parameter to evaluate the whole plant efficiency, which is calculated in the model as follows:

$$Simulated\ efficiency = (Energy\ absorbed\ by\ the\ receiver) / (DNI \times S_h \times N_h) \quad (8)$$

The different sources of efficiency loss in a solar field, as mentioned in the previous section, are considered by the model, where a quite low reflectivity of heliostat due to dust deposition on the mirrors and a heat loss in the receiver based on the feedback of previous campaigns are used in the model. During a relatively stable period, the simulated efficiency is compared with that calculated by the energy transfer from incident solar irradiation to enthalpy of steam (Fig. 5), based on the measured data from the campaign:

$$Mesured\ efficiency = (Q_s \times H_s - Q_w \times H_w) / (DNI \times S_h \times N_h) \quad (9)$$

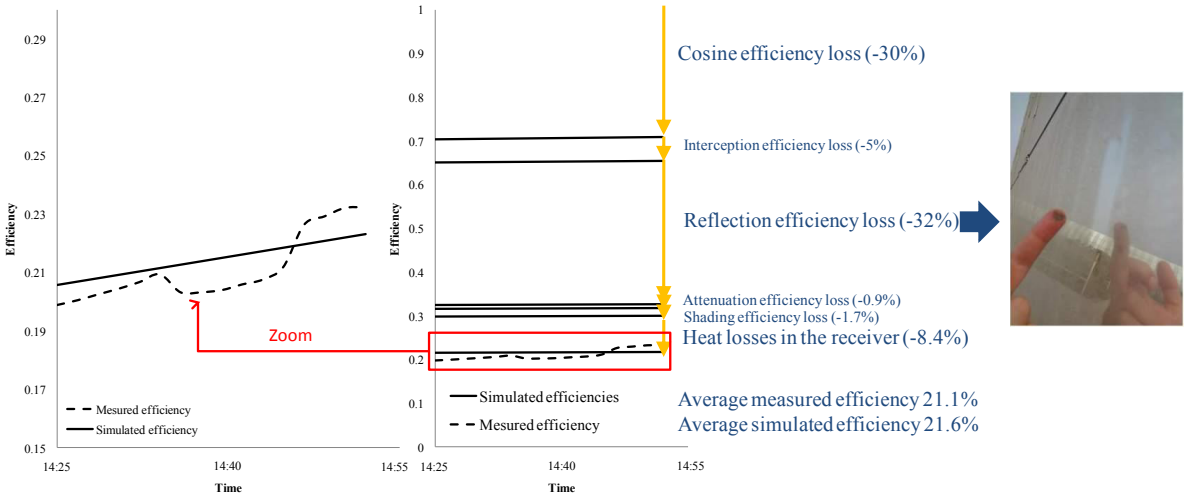

Fig. 5. Comparison between simulated efficiency and measured efficiency for solar field and receiver.

The measured efficiency varies slightly due to the system inertia in response to the DNI evolution, feed water flow rate fluctuation and the automatic disconnection of several heliostats due to communication problem during this period. The average efficiency is around 21%, which meets the expectation because of the low reflectivity of heliostats due to the dust deposition and low DNI level around 550 W/m^2 caused by the clouds passage during the campaign.

5.2. Receiver and power block model

The simulation results for the global model constituted by the solar field, the receiver and the power block are presented (Fig. 6). A relatively stable period of approximately half an hour was selected for this simulation after the turbine rotation and electricity production stabilized from 14:25 to 14:55. The simulation results are compared to the real data obtained from the campaign. During this period, besides a progressive decrease of DNI, only the opening of the main steam valve and the valve before the turbine varies, which is taken into account in the model.

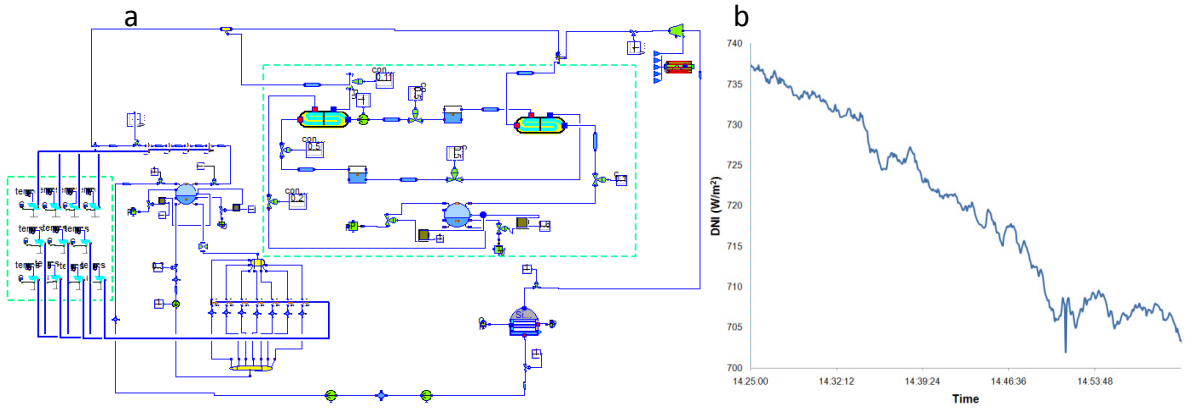

Fig. 6. (a) Model structure including the heliostat and the receiver system, storage system and power block. (b) DNI evolution during the stable phase.

Considering that the main tower was under construction at the time of the campaign, the receiver was installed on a temporary tower, which is located on the west side of the main tower (Fig. 7 a). Therefore the flux distribution is not symmetrical and the heat spot was deviated to the west, which is also confirmed by the simulation result obtained from Soltrace® (Fig. 7 b), causing the overheating of superheater 3, evaporator 6 and to a lower degree, superheater 2. Besides, due to the deviation of the heat spot, no superheating of the steam is observed in the superheaters 1 and 4 based on the campaign feedback, in which the temperature of superheater 1 and 4 equals, respectively, to that of evaporators and superheater 3 (Fig. 8). The main simulation results are in good agreement with the campaign measurements for the period considered (Table 1). The steam mass flow is similar (0.43 kg/s measured vs 0.44 simulated) as well as the evaporator and superheater wall temperatures. It is worth mentioning that the superheater temperature in the campaign is the average value measured by 4 sensors, three of which are located at the back of superheater tubes and only one of which is installed in the front receiving the direct solar irradiation. Besides, the average pressure and temperature in the drum from the campaign feedback is about 12.2 bar and 192.7°C, which is in agreement with the values predicted by the model (12.7 bar and 194.0 °C). The model results for the steam temperature are slightly higher than the experimental ones, but the gap is low compared to the accuracy of measurements.

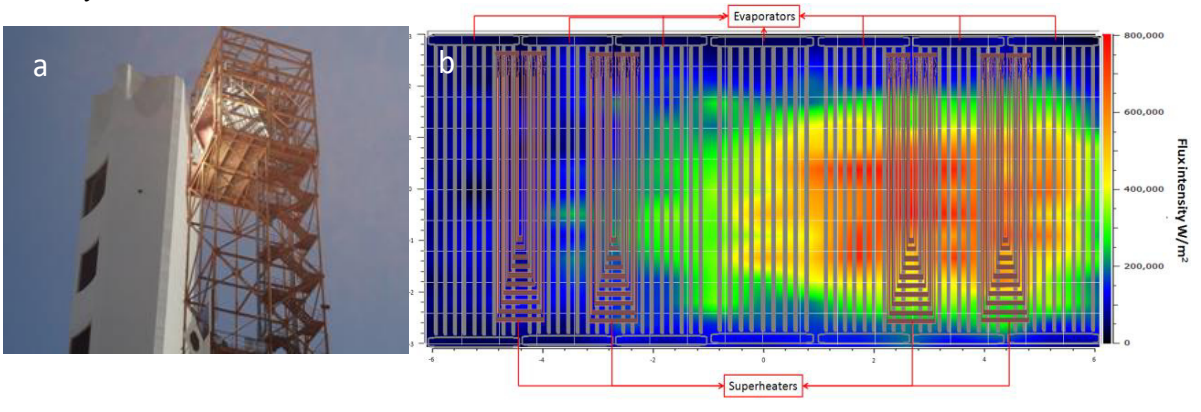

Fig. 7. (a). Two towers in the demo plant. (b). Flux distribution on evaporator and superheater panels.

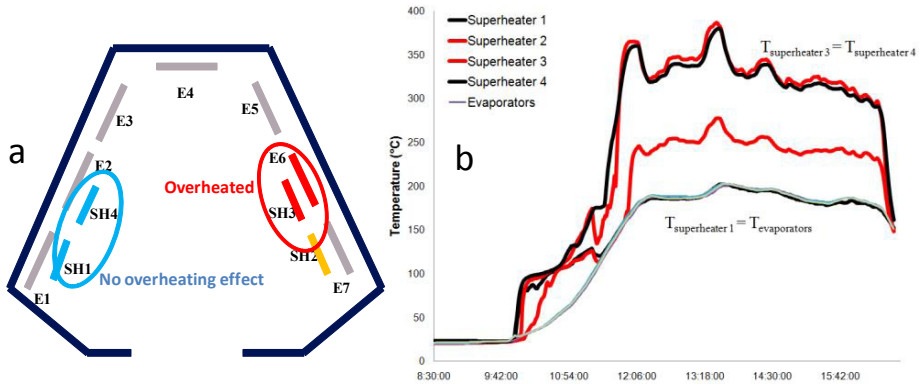

Fig. 8. (a) heat spot deviation in the receiver. (b) Evolution of temperature of superheaters and evaporators during the campaign.

Table 1. Comparison of campaign data and simulation results (average for the period considered).

Parameters	*Campaign results*	*Simulation results*	*Error*
wall T of superheater 1 (°C)	*190.2*	*191.9*	*0.89%*
wall T of superheater 2 (°C)	*242.6*	*245.7*	*1.28%*
wall T of superheater 3 (°C)	*323.2*	*326.8*	*1.11%*
wall T of superheater 4 (°C)	*319*	*322.3*	*1.03%*
wall T of evaporator #1 (°C)	*192.8*	*195.2*	*1.24%*
T in the drum (°C)	*192.7*	*194*	*0.67%*
P in the drum (bar)	*12.2*	*12.7*	*4.10%*
steam flow rate (kg/s)	*0.43*	*0.44*	*2.33%*
P before the turbine (bar)	*6.9*	*8.1*	*17.39%*
Pressure loss between drum and before the turbine (bar)	*5.3*	*4.6*	*13.21%*

The dynamic behaviour of the parameters is also considered. The steam flow rate calculated by the model corresponds well to the measured one during the campaign. The evolution of the superheater wall temperature obtained by the model also shows well the decreasing tendency of wall temperature because of the decreasing DNI (Fig. 9). The reason of a departure in Fig 9b is caused by the fact the DNI was measured by a meteorologic station not far from the solar field instead of in the solar field. Considering the continuously passing clouds during the campaign, the DNI measured could be overestimated. Besides, with a stable flow rate of 0.43 kg/s, an average pressure loss of 5.3 bar from the drum to the turbine inlet is observed, which is slightly higher than the model result of 4.6 bar. This could be explained because the model does not consider yet the pressure drop related to the pipe bend in this section. The mechanical power produced by the turbine, unfortunately, is not measured during the campaign, and, therefore, cannot be compared with the simulated result of 140 kW, which is relatively low compared with the turbine rated power of 1.5 MW. The future test campaigns will be carried out under a higher DNI, heliostat reflectivity and feed water flow rate in order to carry on with the improvement of the model and of the system efficiency.

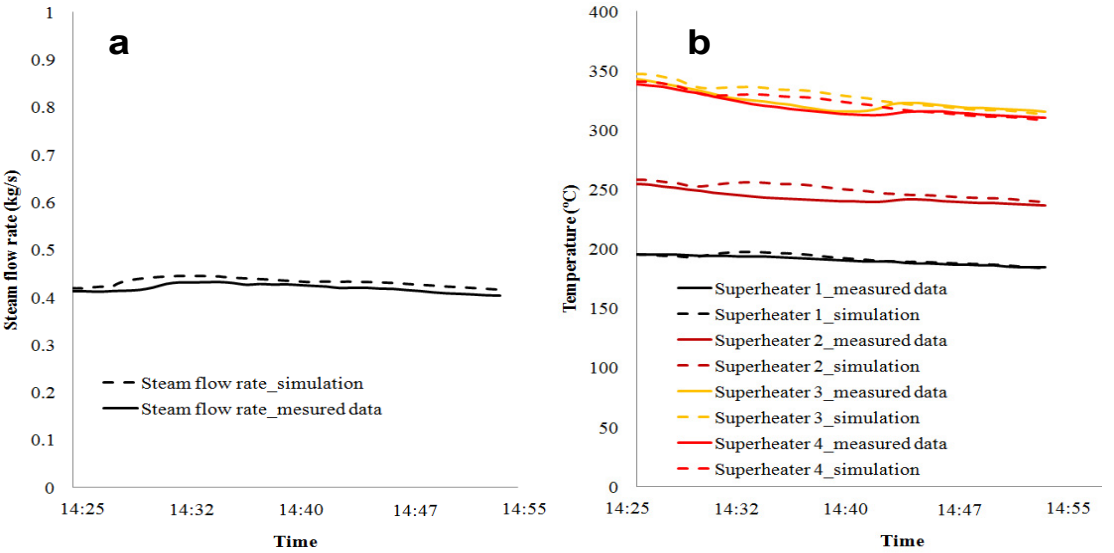

Fig. 9. (a) Evolution of steam flow rate from the campaign feedback and model calculation. (b) Evolution of superheater wall temperature from the campaign feedback and model calculation.

6. Conclusion

A first version of a dynamic model of the Badaling CSP plant has been established, including the heliostat, receiver system and power block. First simulations were carried out and the results were compared to the measured data from this campaign. The evolution of the key parameters in the receiver system fits well with the campaign feedback, which shows the interest of the model as a verification platform for the power system design, support to operation and detection of deviations from normal operation (such as, heat spot deviation in the receiver). The solar field layout method gives good results, in agreement with the real layout of the heliostats in the Badaling power plant. For the receiver and power block, similar average values and trend were obtained. However, in order to increase the accuracy of the model, further improvements are still required regarding the heat losses and axial heat transfer etc....

References

[1] Manteau, G. Centrale experimentale Themis - Dimensionnement economique du stockage et de l'apport en fonction de l'utilisation. Report of Electricite de Fracne; 1978.
[2] Ferriere, A. and Bonduelle, B. Development of an optical control strategy for the Themis solar plant: Part IdThemis transient model. Journal of Solar Energy Engineering 1989; 111: 298-303.
[3] Xu, E.S., Wang, Z.F., Gao, W. and Zhuang J.Y. Dynamic simulation of thermal energy storage system of Badaling 1 MW solar power tower plant. Renewable Energy 2012; 39: 455-462.
[4] Yu, Q., Wang, Z.F., Xu, E.S., Li, X. and Guo, M.H. Modeling and dynamic simulation of the collector and receiver system of 1MWe DAHAN solar thermal power tower plant. Renewable Energy 2012; 43: 18-29.
[5] Siala, F.M.F. and Elayeb, M.E. Mathematical formulation of a graphical method for a no-blocking heliostat field layout. Renewable Energy 2001; 23: 77-92.
[6] Zhang H.L., Wang, Z.F., Wei, X.D. and Lu, Z.W. Design of Heliostats Field for Scale of 1MW Solar Power. Procedia Environmental Sciences 2011; 11: 1164-1170.
[7] Garcia, P., Ferriere, A. and Bezian, J.J. Codes for solar flux calculation dedicated to central receiver system applications: a comparative review 2008; 82: 189-197.